10.24425/119083

Archives of Control Sciences
Volume 28(LXIV), 2018
No. 1*, pages 155–183*

A robust smooth controller for a unicycle-like robot

DARIUSZ PAZDERSKI

In this paper, a stabilizer dedicated for a unicycle-like robot is considered. The proposed smooth control law ensures the global boundedness of position and orientation trajectories to a neighbourhood of the desired point with an arbitrarily selected radius and it is robust to bounded additive measurement noises. The controller consists of a smooth hybrid navigation algorithm and a smooth feedback based on the transverse function approach. The stability proof, simulation and experimental results illustrating properties of the algorithm are discussed.

Key words: transverse functions, nonholonomic system, control motion task, Lie group, navigation vector fields, smooth feedbacks

1. Introduction

Navigation and control of mechanical systems subject to nonintegrable velocity constraints constitute one of the fundamental issues in mobile robotics. It is well known that nonholonomic systems cannot be stabilized by means of a classic smooth time-invariant feedback, [2]. In order to overcome this obstruction, one can apply discontinuous controllers which are known as relatively simple and efficient solutions providing a suitable transient response of a closed-loop system, at least in the nominal case, [16]. Simultaneously, discontinuous feedbacks are heavily prone to bounded disturbances including a measurement noise that may considerably deteriorate a controller performance near singular points, [10]. Another control approach is based on the application of smooth time-dependent asymptotic stabilizers which are usually less sensitive to uncertainties and disturbances. However, they exhibit unsatisfactory convergence rate and manifest usually highly oscillatory transient states.

Taking into account limitations of fundamental classes of stabilizers, it is clear that a robust stabilization of perturbed nonholonomic systems is an important issue. This problem has been already discussed in the robotics literature, cf. [1, 5, 7, 14, 24–26] and [23]. However, most of the cited works deal with discrete and discontinuous techniques. It turns out that the design of a robust smooth

D. Pazderski is with Poznań University of Technology, Institute of Automation and Robotics, ul. Piotrowo 3a 60-965 Poznań, Poland. E-mail: dariusz.pazderski@put.poznan.pl.

Received 26.01.2017. Revised 9.02.2018.

closed-loop algorithm which meets additional criteria and practically motivated properties such as short transient states and a non oscillatory response, is a challenging task. In [13] a method of unifying two types of controllers using non-differentially and smooth state feedbacks is outlined. This algorithm is based, however, on a heuristic rule and no formal stability proof is given.

In this work, we propose a new control method dedicated for a unicycle robot which involves the synthesis of a *smooth navigation* (possibly violating nonholonomic constraints) and a *smooth dynamic feedback* that approximately decouples the nonholonomic kinematics. The task of the navigation algorithm is to generate instantaneous directions in the phase space using holonomic and nonholonomic strategies which are smoothly switched in the prescribed set.

The holonomic smooth navigation strategy can be naturally employed to avoid singularity at the desired point. Additionally, it can provide a robustness to bounded uncertainties including a noise corrupting the measurement of a robot posture. To accomplish the nonholonomic navigation, a method using vector fields with the nonholonomic projection introduced by Lopes and Koditschek is used, [11] (a similar technique is applied, among others, in [12, 19]). Based on Lyapunov-like stability analysis, it is formally shown that a combination of two navigation techniques taking advantage of so-called compatible vector fields makes it possible to obtain the asymptotically stable closed-loop system.

Due to the fact that the navigator in a general case produces velocities which can violate nonholonomic constraints, the obtained trajectory in the configuration space cannot be directly followed by a robot with the unicycle-like kinematics. To overcome this obstruction, we apply the control method based on the transverse functions approach, [15]. The designed controller is used to approximately decouple the nonholonomic kinematics and is unified with the proposed smooth navigator such that the latter governs reference trajectory of *virtual omnidirectional kinematics*, while the nonholonomic robot approximates it with the desired accuracy.

It is worth emphasizing that the control concept based on an approximation of infeasible directions in the phase space is not new in mobile robotics. However, typically it is applied using off-line global planning or iterative local methods, [3, 4, 6, 9, 27]. Conversely, the algorithm proposed in this work is based on other techniques since it is defined in the continuous time domain and takes advantage of a smooth feedback.

The paper is organized as follows. In Section 2 basic notation and fundamental knowledge are outlined. Section 3 covers the presentation of two types of navigation algorithms taking into account robustness issues. In the next section, a new smooth navigation algorithm is proposed and the formal stability analysis is provided. Section 5 is focused on the controller which decouples the unicycle kinematics. Next, the structure of the controller with the navigator is considered. In order to demonstrate the performance of the developed algorithm numerical

simulations for navigation methods and the whole control system are conducted. Additionally, experimental results using a laboratory robot are discussed in Section 6. Section 7 concludes the paper.

2. Preliminaries

2.1. Selected kinematics on SE(2)

Let $g = [x\ y\ \theta]^\top$ denote a planar configuration describing the position and orientation of a robot body. Simultaneously, it is assumed that g is an element of Lie group $G \simeq \mathrm{SE}(2)$ with the group operation defined by

$$\forall g, h \in G,\ gh := g + \begin{bmatrix} R(g_\theta) & 0 \\ 0 & 1 \end{bmatrix} h, \tag{1}$$

where $R \in \mathrm{SO}(2)$ is the planar rotation matrix. The neutral element of G is defined by $e = 0$ while the inverse element of $g \in G$, denoted by g^{-1}, satisfies: $g^{-1}g = gg^{-1} = e$.

It is well known that for any Lie group G its tangent space is determined by Lie algebra $\mathfrak{g}$. Here, it is assumed that basis of this algebra is represented in the matrix form as

$$X(g) = \begin{bmatrix} \cos\theta & 0 & -\sin\theta \\ \sin\theta & 0 & \cos\theta \\ 0 & 1 & 0 \end{bmatrix}, \tag{2}$$

while i^{th} column X_i of X is the independent left-invariant vector field on G, namely the following relation holds

$$\forall g,h \in G, \quad dl_g(h)X_i(h) = X_i(gh), \tag{3}$$

where $dl_g(h)$ stands for derivative of left translation $l_g(h) = gh$ evaluated at h.

Employing the Lie algebra basis, one can naturally define the following planar kinematics

$$\Sigma_O :\ \dot{g} = X(g)\eta, \tag{4}$$

where $\eta = [\eta_1\ \eta_2\ \eta_3]^\top \in \mathbb{R}^3$ denotes a vector of tree independent control inputs – cf. Fig. 1. Since X is invertible from definition, it can be concluded that the phase space of system Σ_O is not constrained. Therefore we call Σ_O as *omnidirectional kinematics*.

Further, we consider that system (4) is subject to the following Pfaffian constraint

$$A(g)\dot{g} = 0, \tag{5}$$

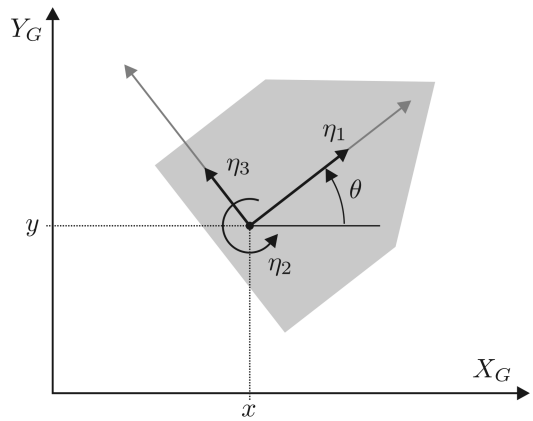

Figure 1: Omnidirectional planar robot with kinematics described by (4) – η_1 and η_3 denote longitudinal and lateral components of linear velocity, respectively, while η_2 is angular velocity

where $A(g) = [-\sin\theta \ \cos\theta \ 0]^\top \in \mathbb{R}^{1\times 3}$ is a constraint matrix. Incorporating this constraint to kinematics (4) implies that $\eta_3 \equiv 0$. Then, assuming that $u \in [u_1 \ u_2]^\top \in \mathbb{R}^2$ denotes an input, and $C = [I \ 0]^\top \in \mathbb{R}^{3\times 2}$, where $I \in \mathbb{R}^{2\times 2}$ is the identity matrix, we obtain the unicycle-like kinematics defined as follows

$$\Sigma_U : \ \dot{g} = X(g)Cu. \tag{6}$$

Equivalently, (6) can be naturally decomposed into the following subsystems describing position and orientation kinematics

$$\dot{p} = X_p(\theta)u_1, \tag{7}$$

$$\dot{\theta} = u_2, \tag{8}$$

where $X_p(\theta) = [\cos\theta \ \sin\theta]^\top$. Since (6) is a differentially flat system with flat output p, orientation variable θ can be explicitly computed based on trajectory $p(t)$ and its time derivative. Taking into account that the last column in A is zero one can rewrite constraint (5) in terms of linear velocity $\dot{p}$ as follows

$$A_p(\theta)\dot{p} = 0, \tag{9}$$

where $A_p(\theta) = [-\sin\theta \ \ \cos\theta]^\top \in \mathbb{R}^{1\times 2}$. One can easily check that (9) holds for

$$\theta = \operatorname{atan2}(\zeta\dot{y}, \zeta\dot{x}), \tag{10}$$

where $\operatorname{atan2}(\cdot,\cdot)$ stands for the two-argument inverse tangent and $\zeta \in \{-1, 1\}$ is a parameter. Additionally, we can distinguish the singular case for which $\dot{p} = 0$ – then constraint (9) is trivially satisfied for any $\theta \in \mathbb{S}^1$.

A key property of control systems on Lie groups is related to a symmetry of configuration and phase spaces. In the considered case this symmetry is manifested in the form of coordinate transformations which preserves kinematic equation. Accordingly, assuming that $\widetilde{g} = g_d^{-1} g$ denotes an error between point $g_d = \text{const} \in G$ and g, it follows that kinematics Σ_O and Σ_U can be defined by: $\dot{\widetilde{g}} = X(\widetilde{g})\eta$ and $\dot{\widetilde{g}} = X(\widetilde{g})Cu$, respectively. Further, we take advantage of this property assuming without loss of generality that the desired point is attached at the origin, namely $g_d = e$. Moreover, in this paper Lie group G is employed in order to design a motion controller investigated in section 5.

2.2. Prototype trajectory in $\mathbb{R}^2$

Consider the following continuous dynamics in $\mathbb{R}^2$

$$\dot{\xi} = Y_v(\xi), \tag{11}$$

where $\xi \in \mathbb{R}^2$ and $Y_v = Y_{v_x}\dfrac{\partial}{\partial x} + Y_{v_y}\dfrac{\partial}{\partial y}$ is a vector field with components Y_{v_x} and Y_{v_y} being functions $\mathbb{R}^2 \to \mathbb{R}$.

Next, we assume that the following properties hold.

A1: Vector field Y_v is smooth at least on open set $\mathbb{R}^2 \setminus \{0\}$.

A2: For any $\xi \in \mathbb{R}^2$ there exists the following positive definite function

$$V = \xi^\top P \xi, \tag{12}$$

a such that its time derivative satisfies

$$\dot{V} \leqslant -\xi^\top Q \xi \tag{13}$$

with $P, Q \in \mathbb{R}^{2\times 2}$ being positive definite and symmetric constant matrices.

A3: Derivative $\dfrac{\partial Y_v}{\partial \xi}$ can be bounded as follows

$$\forall \xi \in \mathbb{R}^2, \quad \left\| \frac{\partial Y_v}{\partial \xi} \right\|_F < M, \tag{14}$$

where $\|\cdot\|_F$ denotes the matrix Frobenius norm and $M > 0$ is a constant.

Additionally, we formulate the following optional assumption with respect to Y_v:

A4: Let $\varphi^{Y_v}(\xi_0, t) = \xi(t)$ denote the flow of vector field Y_v with initial condition $\xi_0 = \xi(0)$ a such that the following relationship is satisfied:

$$\forall \xi(0) \in \mathbb{R}^2 \setminus \{0\}, \quad \lim_{t\to\infty} \dot{\xi}_y(t)/\dot{\xi}_x(t) = 0. \tag{15}$$

From assumption A2 follows that system (11) is globally asymptotically stable at equilibrium $\xi = 0$. As a result of A4, trajectory $\xi_y(t)$ converges to zero faster than $\xi_x(t)$. Thus, trajectory $\xi(t)$ becomes tangent to X_G-axis of the inertial frame as time goes to infinity – cf. Fig. 2. Notice, that the similar property is required in [12, 19] and [18].

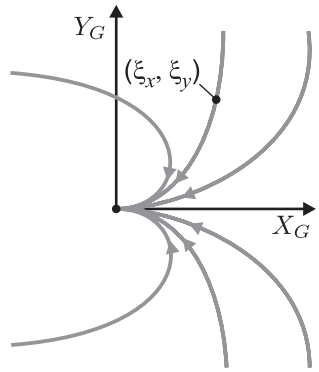

Figure 2: Set of flows of vector field Y_v which satisfies assumptions A1–A4

Vectors fields Y_v satisfying conditions A1, A2 and A3 constitute a class of *compatible navigation vector fields* on $\mathbb{R}^2$. When they also satisfy A4, we call them *nominal nonholonomic navigation vector fields*.

3. Basic navigation algorithms

Let $g_v = \left[p_v^\top \theta_v\right]^\top$ denote the configuration of omnidirectional kinematics (4) with input η. We assume that a navigation algorithm is defined by a continuous (or even smooth) feedback and governs trajectory g_v which is a solution of the following differential equation

$$\dot{g}_v = \overline{Y}(g_v), \tag{16}$$

where $\overline{Y} \in \mathbb{R}^3$ denotes a vector field. Input η which defines instantaneous velocities in the local frame (cf. Fig. 1) can be computed as follows

$$\eta = X^{-1}(g_v)\overline{Y}(g_v). \tag{17}$$

In this section we consider two propositions of navigation strategies in sequel. The first one is based on a smooth feedback which produces arbitrarily trajectory $g_v(t)$. The second strategy takes advantage of a non smooth nonholonomic navigation for which phase constraint (5) is satisfied and trajectory $g_v(t)$ is admissible for the unicycle kinematics.

3.1. Holonomic navigator

In order to design a holonomic navigator we consider vector field $Y_v = Y_h$ for which assumptions A1, A2 and A3 hold. Moreover, we assume that Y_h is a smooth vector field on $\mathbb{R}^2$ (including the origin). In such a case one can easily replicate prototype position trajectory ξ. Recalling (11) one has

$$\dot{p}_v = Y_h(p_v). \tag{18}$$

From assumption A2 follows that there exists function

$$V = p_v^\top P p_v \tag{19}$$

which is a Lyapunov function for system (18) with time derivative

$$\dot{V} = 2p_v^\top P Y_h(p_v) \leqslant -p_v^\top Q p_v \leqslant -\lambda \|p_v\|^2, \tag{20}$$

where

$$\lambda = \min\{\mathrm{eig}(Q)\}. \tag{21}$$

Hence, trajectory $p_v(t)$ converges to zero exponentially.

Notice that orientation θ_v does not affect closed-loop dynamics (18) which makes it possible to control θ_v in an arbitrary way. In order to stabilize the orientation, one can, for example, apply the following basic feedback

$$\dot{\theta}_v = -k_\theta \theta_v \tag{22}$$

which ensures that $\theta_v(t)$ tends to zero for any $k_\theta > 0$.

3.2. Nonholonomic navigator

Assume that trajectory $g_v(t) \in G$ computed by the navigation algorithm is admissible for the unicycle-like kinematics, namely $g_v(t)$ satisfies the Pfaffian constraint defined by (5).

We design position trajectory p_v taking advantage of prototype trajectory ξ which is a flow of nonholonomic vector field $Y_v = Y_{nh}$ satisfying assumptions A1, A2, A3 and A4. It is important to emphasise that the latter assumption is critical for the discussed nonholonomic navigation. It implies that $\xi(t)$ converges to the origin in such a way that vector field Y_{nh} becomes collinear with $\dfrac{\partial}{\partial x}$ as time goes to infinity (to be more precise, point $\xi = 0$ where Y_{nh} vanishes is excluded from the assumption).

As a result of constraint (9), one cannot straightforwardly assume that $p_v = \xi$ is a feasible trajectory for any $\theta_v \in \mathbb{S}^1$. According to (10), constraint (9) is satisfied for $\xi \neq 0$ when $\theta_v = \theta_{nh}$, where

$$\theta_{nh} = \mathrm{atan2}(\zeta Y_{nh_y}, \zeta Y_{nh_x}) \tag{23}$$

with Y_{nh_x}, Y_{nh_x} being components of vector field Y_{nh}.

In order to overcome this issue, we employ so-called *nonholonomic projection* which maps any bounded vector field on a feasible velocity, [11]. In the considered case we define a map $\mathbb{R}^2 \to W_p$, where $W_p := \{w \in \mathbb{R}^2 : A_p(\theta_v)w = 0\}$ denotes a set of feasible velocities for the given constraint. Recalling position kinematics (7) the nonholonomic projection can be defined as follows

$$\dot{p}_v = H(\theta_v)\dot{\xi}, \tag{24}$$

where

$$H(\theta_v) := X_p(\theta_v)X_p(\theta_v)^\sharp \in \mathbb{R}^{2\times 2} \tag{25}$$

is the *nonholonomic projection matrix*, while

$$X_p(\theta_v)^\sharp := (X_p(\theta_v)^\top X_p(\theta_v)^{-1}X_p(\theta_v)^\top$$

denotes the Moore-Penrose left pseudoinverse.

Using (11) with $Y_v = Y_{nh}$ in (24) we obtain

$$\dot{p}_v = H(\theta_v)Y_{nh}(p_v), \tag{26}$$

Following (26) we propose the nonholonomic navigation feedback.

Proposition 1 (Nominal nonholonomic navigator) *Trajectory $g_v(t)$ of dynamic system defined by* (26) *and the following differential equation*

$$\dot{\theta}_v := -k_\theta \widetilde{\theta}_v + \dot{\theta}_{nh}, \tag{27}$$

with $\widetilde{\theta} = \theta_v - \theta_{nh}$, $k_\theta > 0$ converges asymptotically to zero for any $p_v(0) \neq 0$ and $\theta_v(0) \in \mathbb{S}^1$.

Proof Consider function V given by (19). Taking time derivative of V gives $\dot{V} = 2p_v^\top PH(\theta_v)Y_{nh}(p_v)$. Then adding and subtracting term $2p_v^\top PY_{nh}(p_v)$ in $\dot{V}$ one has

$$\begin{aligned}\dot{V} &= 2p_v^\top PY_{nh}(p_v) - 2p_v^\top PY_{nh}(p_v) + 2p_v^\top PH(\theta_v)Y_{nh}(p_v)\\ &= 2p_v^\top PY_{nh}(p_v) + 2p_v^\top P\left(H(\theta_v) - I\right)Y_{nh}(p_v).\end{aligned} \tag{28}$$

Following assumption A2 and relations (12)-(13) one can write that $\dfrac{d}{dt}\xi^\top P\xi = 2\xi^\top PY_{nh}(\xi) \leqslant -\xi^\top Q\xi$. As a result, the following bound can be written

$$2p_v^\top PY_{nh}(p_v) \leqslant -p_v^\top Qp_v. \tag{29}$$

Using (29) in (28) yields

$$\dot{V} \leqslant -p_v^\top Qp_v - 2p_v^\top P\left(I - H(\theta_v)\right)Y_{nh}(p_v). \tag{30}$$

Computing $H(\theta_v)$ from (25) one has

$$I - H(\theta_v) = \begin{bmatrix} \sin^2\theta_v & -\sin\theta_v\cos\theta_v \\ -\sin\theta_v\cos\theta_v & \cos^2\theta_v \end{bmatrix} = \begin{bmatrix} 0 & -\sin\theta_v \\ 0 & \cos\theta_v \end{bmatrix} R^\top(\theta_v). \quad (31)$$

Taking advantage of (23) and recalling definition of X_p one can show that $Y_{nh}(p_v) = \zeta \|Y_{nh}(p_v)\| X_p(\theta_{nh})$. Using this relation and formula (31) one can write

$$\begin{aligned}(I - H(\theta_v))\, Y_{nh}(p_v) &= \zeta \|Y_{nh}(p_v)\| \begin{bmatrix} 0 & -\sin\theta_v \\ 0 & \cos\theta_v \end{bmatrix} R^\top(\theta_v) X_p(\theta_{nh}) \\ &= \zeta \|Y_{nh}(p_v)\| \begin{bmatrix} \sin\theta_v \\ -\cos\theta_v \end{bmatrix} \sin\widetilde{\theta}_v. \end{aligned} \quad (32)$$

Substituting (32) in (30) gives

$$\dot{V} \leqslant -p_v^\top Q p_v - 2\zeta \|Y_{nh}(p_v)\| p_v^\top P \begin{bmatrix} \sin\theta_v \\ -\cos\theta_v \end{bmatrix} \sin\widetilde{\theta}_v. \quad (33)$$

The first term in (33) can be bounded as follows: $-p_v^\top Q p_v \leqslant -\lambda \|p_v\|^2$, where λ is defined by (21). Referring to (29) it can be concluded that expression $p_v^\top P Y_{nh}(p_v)$ is quadratic in terms of p_v. Consequently, relationship $2\zeta \|Y_{nh}(p_v)\| p_v^\top P \begin{bmatrix} \sin\theta_v \\ -\cos\theta_v \end{bmatrix}$ in (33) can be bounded as follows

$$2 \left| \zeta \|Y_{nh}(p_v)\| p_v^\top P \begin{bmatrix} \sin\theta_v \\ -\cos\theta_v \end{bmatrix} \right| \leqslant \alpha \|p_v\|^2, \quad (34)$$

where $\alpha > \lambda$ is a constant. Following the given simplifications $\dot{V}$ satisfies

$$\dot{V} \leqslant \left(-\lambda + \alpha |\sin\widetilde{\theta}_v| \right) \|p_v\|^2. \quad (35)$$

Now we consider the closed-loop orientation dynamics. From (27) one can conclude that

$$\widetilde{\theta}_v(t) = \widetilde{\theta}_v(0) \exp(-k_\theta t). \quad (36)$$

As a result, $\sin\widetilde{\theta}_v$ converges to zero which implies that perturbation term in (33) given by $\alpha|\sin\widetilde{\theta}_v|$ is bounded and decays exponentially. Hence, there exists time instant $\tau > 0$ such that

$$\forall t > \tau, \qquad \lambda > \alpha |\sin\widetilde{\theta}_v(t)|. \quad (37)$$

Consequently, at $t > \tau$ derivative $\dot{V}$ becomes negative and V converges to zero. Then, based on definition of V one can prove that

$$\lim_{t\to\infty} p_v(t) = 0. \tag{38}$$

Taking into account (38), (26) and recalling that Y_{nh} is bounded for bounded p_v, one has $\lim_{t\to\infty} \dot{p}_v(t) = 0$. Recalling assumption A4, relation (15) and (23) one concludes that

$$\lim_{t\to\infty} \theta_{nh}(t) = 0 \text{ or } \lim_{t\to\infty} \theta_{nh}(t) = \pi. \tag{39}$$

In order to ensure that $\lim_{t\to\infty} \theta_{nh}(t) = 0$ one has to select ζ in (23) such that $for\ t > T, \zeta\dot{x}_v > 0$, where $T > 0$ is some constant. Following (36) it can be shown that

$$\lim_{t\to\infty} \theta_v(t) = 0. \tag{40}$$

To complete the proof, we need to confirm that derivative $\dot{g}_v$ is bounded. Recalling (26) and taking into account that $p_v \in \mathscr{L}_\infty$ it can be found that $\dot{p}_v \in \mathscr{L}_\infty$. Investigating boundedness of $\dot{\theta}_v$ from (27) one can see that $\widetilde{\theta}_v \in \mathscr{L}_\infty$. Taking advantage of result (91) provided in the Appendix, time derivative $\dot{\theta}_{nh}$ can be computed as follows

$$\dot{\theta}_{nh} = \frac{Y_{nh}^\top}{\|Y_{nh}\|^2} J\dot{Y}_{nh}. \tag{41}$$

Noticing that $\dot{Y}_{nh} = \frac{\partial Y_{nh}}{\partial p_v} Y_{nh}$ one obtains

$$\dot{\theta}_{nh} = \frac{Y_{nh}^\top}{\|Y_{nh}\|} J \frac{\partial Y_{nh}}{\partial p_v} \frac{Y_{nh}}{\|Y_{nh}\|}. \tag{42}$$

Since $\frac{\partial Y_{nh}}{\partial p_v}$ and $Y_{nh}/\|Y_{nh}\|$ are bounded one concludes that $\dot{\theta}_{nh} \in \mathscr{L}_\infty$. More precisely, recalling (14) and noticing that $\|J\|_F = \sqrt{2}$ function $\dot{\theta}_{nh}$ can be bounded as

$$|\dot{\theta}_{nh}| \leqslant \sqrt{2}M. \tag{43}$$

3.3. Sensitivity analysis

Now we assume that a navigation vector field is computed when the configuration is not known perfectly. However, in order to simplify analysis, we consider the case when only position coordinates are affected by bounded disturbances while orientation θ_v can be measured precisely. This simplification can be further justified taking into account that predominant undesirable effects in

the discussed nonholonomic navigation algorithm comes from a noise added to position variables.

To be more precise, we define output $p_v^* \in \mathbb{R}^2$ which describes the measured position of the robot

$$p_v^* = p_v + \delta_p, \tag{44}$$

where $\delta_p \in \mathbb{R}^2$ is a bounded disturbance such that $\|\delta_p\| < \rho$, where $\rho > 0$. Next, we investigate how navigation vector field Y_v is perturbed and introduce the following approximation

$$Y_v(p_v^*) = Y_v(p_v) + \Delta_Y, \tag{45}$$

where $\Delta_Y = \dfrac{\partial Y_v}{\partial p_v}\delta_p + O(\delta_p^2)$ denotes perturbation of navigating vector field. Additionally, referring to assumption A3 the following bound can be established

$$\forall p_v \in \mathbb{R}^2, \quad \|\delta_p\| < \rho, \exists \overline{m} > 0, \|\Delta_Y\| \leqslant \overline{m}. \tag{46}$$

Next, we study how the given uncertainty affects the holonomic navigation algorithm. Defining perturbed version of dynamics (18) and substituting (45) with $Y_v = Y_h$ we have

$$\dot{p}_v = Y_h(p_v^*) = Y_v(p_v) + \Delta_Y. \tag{47}$$

Recalling stability analysis outlined in subsection 3.1, using the same definition of V and taking into account (46), for perturbed system (47) one obtains

$$\dot{V} \leqslant -\lambda\|p_v\|^2 + 2\|\Delta_Y\|\|p_v\| \leqslant -\lambda\|p_v\|^2 + 2\overline{m}\|p_v\|. \tag{48}$$

Since $\dot{V} < 0$ when $\|p_v\| > \dfrac{2\overline{m}}{\lambda}$ one easily concludes that

$$\lim_{t\to\infty} \|p_v(t)\| \leqslant \frac{2}{\lambda}\overline{m}. \tag{49}$$

Further, we discuss the stability of the closed-loop system taking into account the nonholonomic navigator proposed in section 3.2. Referring to (47) and using perturbed vector field one obtains

$$\dot{p}_v = H(\theta_v)Y_{nh}(p_v^*) = H(\theta_v)(Y_{nh}(p_v) + \Delta_Y). \tag{50}$$

Making the similar stability analysis as in proof 3.2 with $V = p_v^\top P p_v$, computing $\dot{V}$ and substituting (50) yields (cf. (30))

$$\dot{V} = 2p_v^\top P Y_{nh}(\theta_v) + 2p_v^\top P(H(\theta_v) - I)Y_{nh}(\theta_v) + 2p_v^\top P H(\theta_v)\Delta_Y. \tag{51}$$

Applying mathematical manipulations discussed in proof 3.2, using (34), defining

$$\forall \theta_v \in \mathbb{S}^1, \quad \exists \beta > \|PH(\theta_v)\|_F \tag{52}$$

and taking into account (46) one can rewrite (51) as follows

$$\dot{V} \leqslant (-\lambda + \alpha |\sin(\theta_v - \theta_{nh}))\, \|p_v\|^2 + 2\beta \overline{m} \|p_v\| \tag{53}$$

It can be easily noticed that (53) is composed of (33) and additive term $2\beta\overline{m}\|p_v\|$. However, in the considered case variable θ_{nh} is not well determined. Recalling definition (23) it is important to emphasise that θ_{nh} is computed for Y_{nh} evaluated at p_v which is not known accurately. In order to overcome this difficulty one can expect that θ_{nh} can be approximated by

$$\theta^*_{nh} = \operatorname{atan2}(\zeta Y_{nh_y}, \zeta Y_{nh_x})|_{p^*_v}. \tag{54}$$

We consider this issue more thoroughly. Similarly to (45), we assume that

$$Y_v(p^*_v) = Y_v(p_v) + \gamma \overline{\Delta}_Y, \tag{55}$$

where $\gamma \in \mathbb{R}$ and $\overline{\Delta}_Y \in \mathbb{R}^2$ is some non-zero perturbation. Then we approximate θ^*_{nh} as follows

$$\theta^*_{nh} = \theta_{nh} + \left.\frac{\partial \theta^*_{nh}}{\partial \gamma}\right|_{\gamma=0} \gamma + O(\gamma^2). \tag{56}$$

Taking into account result (94) presented in the Appendix, it can be concluded that for $Y_v(p_v)$ derivative $\left.\dfrac{\partial \theta^*_{nh}}{\partial \gamma}\right|_{\gamma=0}$ becomes unbounded. Hence, one can notice that distance $|\theta^*_{nh} - \theta_{nh}|$ grows significantly when components of nominal navigating vector field are close to zero. As a result disturbance added to p_v affects orientation control significantly.

In the considered case control feedback (27) can be rewritten as follows

$$\dot{\theta}_v := -k_\theta(\theta_v - \theta^*_{nh}) + \dot{\theta}^*_{nh}. \tag{57}$$

Since terms denoted by $*$ in (57) are computed based on $Y_v(p^*_v)$, they are bounded – cf. result given by (42). In spite of that, the sensitivity of determination of θ^*_{nh} increases rapidly when p_v is in a vicinity of the origin where norm $\|Y_{nh}(p_v)\|$ is small. As a consequence, an equilibrium point for dynamics (57) cannot be determined and the given system is unstable for additive disturbance δ_p in a neighbourhood of zero.

4. Smooth robust navigation algorithm

4.1. Proposition of the algorithm

In order to cope with the singularity of nonhonolonic navigation which leads to extremely high sensitivity to disturbances at neighbourhood of $p_v = 0$, we propose a new smooth hybrid structure.

Here, we take advantage of vector fields Y_h and Y_{nh} which belong to the same class of navigation vector fields and satisfy conditions A1, A2 and A3 for the same proposition of V. A basic idea of a robust feedback used for the navigation purpose comes from the selection of navigation strategies which work efficiently in the defined domains of the configuration (task) space. Taking into account the weakness of nonholonomic navigation in a vicinity of the desired point, it is preferred to employ a smooth feedback in the prescribed neighbourhood. Conversely, when a navigating vector field is well conditioned (for example when the robot is far away from the desired point), it is reasonably to apply nonholonomic navigation in order to improve dynamic response of the closed-loop system and to decrease control effort (the motion in directions determined by Lie brackets in short-time period can be avoided). To guarantee the smoothness of a navigation strategy, we exclude non-smooth switching strategies proposed in some papers. Instead of a hard switching function we consider the following smooth (not analytical) bump-like function

$$\sigma_{c,r}(d) = \begin{cases} \left(1 + \exp \dfrac{4r(d-c)}{(d-c+r)(d-c-r)}\right)^{-1} & \text{for } d \in (c-r, c+r) \\ 0 & \text{for } d \leqslant c-r \\ 1 & \text{for } d \geqslant c+r \end{cases}, \quad (58)$$

where $c \in \mathbb{R}$ and $r \in \mathbb{R}_+$ are parameters which determine boundaries of transition range $(c-r, c+r)$ – cf. also Fig. 3.

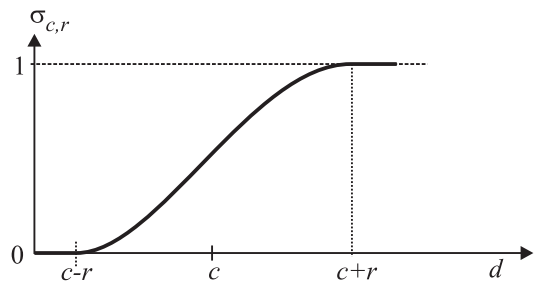

Figure 3: Interpretation of the smooth switching function defined by (58)

Proposition 2 (Smooth robust navigation algorithm) *Assume that the position trajectory is governed by the following equation*

$$\dot{p}_v = \sigma_{c_p,r_p}(V(p_v))H(\theta_v)Y_{nh}(p_v) + (1-\sigma_{c_p,r_p}(V(p_v)))Y_h(p_v), \tag{59}$$

while orientation dynamics satisfies

$$\dot{\theta}_v = -\overline{k}_\theta\,(\theta_v - \theta_d) \tag{60}$$

with $\overline{k}_\theta > K_\theta$ *being positive gain and*

$$\theta_d := \sigma_{c_\theta,r_\theta}(V)\theta_{nh}. \tag{61}$$

Parameters of switching function $c_p, r_p, c_\theta, r_\theta$ *satisfy (cf. Fig. 4):*

$$c_p - r_p > c_\theta - r_\theta > 0. \tag{62}$$

Then, for large enough K_θ *trajectory* $g_v(t)$ *globally and asymptotically converges to zero.*

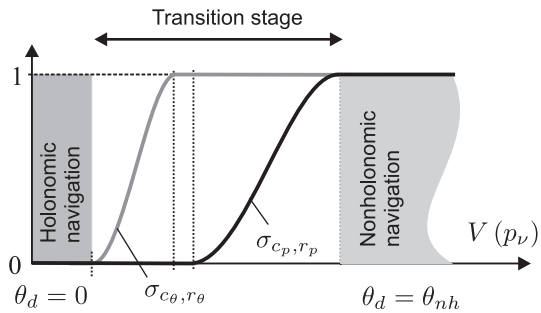

Figure 4: Interpretation of the switching between holonomic and nonholonomic navigation stages

Proof Taking advantage of function (19), computing its time derivative and using (59) one obtains

$$\dot{V} = 2p_v^\top P\dot{p}_v = 2p_v^\top P\left(\sigma_{c_p,r_p}(V)H(\theta_v)Y_{nh}(p_v) + (1-\sigma_{c_p,r_p}(V))Y_h(p_v)\right). \tag{63}$$

Adding and subtracting $\sigma_{c_p,r_p}(V)Y_{nh}(p_v)$ in (63) yields

$$\begin{aligned}\dot{V} =& 2p_v^\top P\left(-\sigma_{c_p,r_p}(V)\,(I-H(\theta_v))\,Y_{nh}(p_v)\right.\\ &\left.+\sigma_{c_p,r_p}(V)Y_{nh}(p_v) + (1-\sigma_{c_p,r_p}(V))Y_h(p_v)\right)\\ =& 2p_v^\top P\left(\sigma_{c_p,r_p}(V)Y_{nh}(p_v) + (1-\sigma_{c_p,r_p}(V))Y_h(p_v)\right)\\ &- 2\sigma_{c_p,r_p}(V)p_v^\top P\,(I-H(\theta_v))\,Y_{nh}(p_v).\end{aligned} \tag{64}$$

Taking advantage of assumption A2 and recalling the compatibility of both navigation vector fields one has

$$\dot{V} \leqslant -p_v^\top Q p_v - 2\sigma_{c_p,r_p}(V) p_v^\top P (I - H(\theta_v)) Y_{nh}(p_v). \tag{65}$$

Next, comparing (63) and (30) one obtains

$$\dot{V} \leqslant \left(-\lambda + \alpha \sigma_{c_p,r_p}(V) |\sin(\theta_v - \theta_{nh}|\right) \|p_v\|^2. \tag{66}$$

Taking into account values of switching function σ_{c_p,r_p} one can rewrite (66) as follows

$$\dot{V} \leqslant \begin{cases} \left(-\lambda + \alpha \sigma_{c_p,r_p}(V) |\sin \widetilde{\theta}_v|\right) \|p_v\|^2 & \text{for } c_p - r_p < V < c_p + r_p \\ \left(-\lambda + \alpha |\sin \widetilde{\theta}_v|\right) \|p_v\|^2 & \text{for } V \geqslant c_p + r_p \\ -\lambda \|p_v\|^2 & \text{for } V \leqslant c_p - r_p \end{cases}. \tag{67}$$

From (67) one can notice that for $V > c_p - r_p$, namely when nonholonomic navigating vector field is considered, a suitable control of orientation θ_v is critical. To be more precise, in the given range of V, variable θ_v should follow trajectory $\theta_{nh}(t)$. Referring to (61) and condition (62) it can be concluded that for $V > c_p - r_p$, $\theta_d = \theta_v$ and control feedback (60) becomes equivalent to $\dot{\theta}_v = -\overline{k}_\theta(\theta_v - \theta_{nh})$. Then, one can consider the following closed-loop system

$$\dot{\widetilde{\theta}}_v = -\overline{k}_\theta \widetilde{\theta}_v + \dot{\theta}_{nh}. \tag{68}$$

Since $\dot{\theta}_{nh}$ satisfies (43), it implies that trajectory $\widetilde{\theta}_v$ is bounded as follows

$$\lim_{t\to\infty} |\widetilde{\theta}_v(t)| \leqslant \epsilon_\theta = \frac{\sqrt{2}M}{\overline{k}_\theta}. \tag{69}$$

It is clear that upper bound ϵ_θ can be adjusted by making gain $\overline{k}_\theta$ large enough. As a result term $\alpha|\sin\widetilde{\theta}_v|$ can be attenuated until $\dot{V} < 0$ – cf. (67). Consequently, there exists finite time instant $\tau > 0$ when value of V becomes below $c_p - r_p$. Then, holonomic vector field Y_h ensures that $p_v = 0$ is the asymptotically stable equilibrium point. Moreover, for $V < c_\theta - r_\theta$, $\theta_d = 0$, cf. (61), and orientation θ_v is governed by: $\dot{\theta}_v = -\overline{k}_\theta \theta_v$. As a consequence, θ_v tends to zero exponentially.

Remark 1 *In* (60) *feedforward term* $\dot{\theta}_d$ *is neglected – cf.* (27). *This is due to the fact that derivative of* θ_{nh} *can lead to higher sensitivity of the proposed strategy to the measurement noise. In order to decrease orientation error* $\widetilde{\theta}_v$ *to an acceptable range, it is required to select gain* $\overline{k}_\theta > K_\theta$ *large enough.*

4.2. Particular selection of navigation vector fields

The selection of navigation vector fields can be made based on assumptions formulated in section 2.2. Now we consider an exemplary choice of such vector fields.

Firstly, the holonomic vector field is proposed as follows

$$Y_h(\xi) = k_v A_h \xi \tag{70}$$

with

$$A_h := -\mathrm{diag}\{1, \beta_v\} \in \mathbb{R}^{2\times 2} \tag{71}$$

being a Hurwitz matrix for any k_v and $\beta_v > 0$. Since vector field Y_h is linear, it trivially satisfies assumptions A1–A3.

Secondly, based on formula (70) the following nonholonomic navigation vector field is defined

$$Y_{nh}(\xi) = Y_h(\xi) - k_v \kappa_v [|\xi_y|\ 0]^\top = -k_v A_{nh}(\xi)\xi, \tag{72}$$

where

$$A_{nh}(\xi) = \begin{bmatrix} 1 & -\kappa_v \mathrm{sgn}(\xi_y) \\ 0 & \beta_v \end{bmatrix} \tag{73}$$

with κ_v being a constant parameter. This vector field satisfies assumptions A1 (it is smooth on a restricted domain) and A3 (its derivative is bounded). Moreover, assumption A2 is also satisfied, since one can select $V(\xi) := \xi^\top \xi$ as a Lyapunov function candidate with time derivative given by

$$\dot{V} = -\xi^\top Q \xi. \tag{74}$$

where

$$Q = k_v \left(A_{nh}(\xi)^\top + A_{nh}(\xi) \right) = k_v \begin{bmatrix} 2 & -\kappa_v \mathrm{sgn}(\xi_y) \\ -\kappa_v \mathrm{sgn}(\xi_y) & 2\beta_v \end{bmatrix}. \tag{75}$$

One can easily prove that $Q \succ 0$ for $\kappa_v^2 < 4\beta_v$ and

$$\lambda = k_v \left(\beta_v + 1 - 2\sqrt{(\beta_v - 1)^2 + \kappa_v^2} \right). \tag{76}$$

In order to check if assumption A4 holds, we look for a solution of differential equation $\dot{\xi} = -A_{nh}(\xi)$ and obtain the following result

$$\xi_x(t) = \begin{cases} \left(\xi_{x0} - \kappa_v \mathrm{sgn}(\xi_{y0}) t\right) e^{-t}, & \text{for } \beta_v = 1 \\ \left(\xi_{x0} - \dfrac{\kappa_v \mathrm{sgn}(\xi_{y0})}{1-\beta_v} \xi_{y0}\right) e^{-t} + \dfrac{\kappa_v \mathrm{sgn}(\xi_{y0})}{1-\beta_v} \xi_{y0} e^{-\beta_v t}, & \text{for } \beta_v \neq 1 \end{cases} \tag{77}$$

and

$$\xi_y(t) = \xi_{y0} e^{-\beta_v t}, \tag{78}$$

while $\xi_{x0} = \xi_x(0)$ and $\xi_{y0} = \xi_y(0)$ denote initial conditions. Computing $\dot{\xi}_x$ and $\dot{\xi}_y$ from (77) and (78), respectively it can be proved that assumption A4 defined by formula (15) is satisfied for $\beta_v \geqslant 1$.

5. Control algorithm

The navigation strategy proposed in section 4 determines instantaneous velocity $\dot{g}_v$ which does not satisfies nonholonomics constraint (5) in some vicinity of the desired point. Therefore this trajectory cannot be followed directly by a unicycle-like robot. In order to cope with this issue, it is necessary to convert infeasible movements into manoeuvres which can be executed by the controlled nonholonomic robot.

Since the proposed navigation algorithm is based on the smooth feedback, it is expected that a local motion controller should also ensure the smoothness property. Here, we take advantage of the *transverse functions approach* in order to design a motion controller which make it possible to approximate any bounded trajectory in the configuration space. In such a case the trajectory $g_v(t)$ computed for the omnidirectional kinematics becomes virtually coupled with trajectory $g(t)$ of the controlled nonholonomic robot.

Let $f_T : \mathbb{S}^1 \to G$ denote a smooth and bounded function which satisfies

$$\forall \alpha \in \mathbb{S}^1, \ \mathrm{rank} W(\alpha) = 3 \tag{79}$$

while $W(\alpha) := \left[X(f_T) C \ \ \dfrac{\partial f_T}{\partial \alpha} \right] \in \mathbb{R}^{3\times 3}$ and $\|f_T\| \leqslant \delta$. For unicycle kinematics (6) transversality condition (79) is satisfied, for example, by the following function

$$f_T(\alpha) := \left[\varepsilon_1 \sin\alpha \ \ \overline{\varepsilon}_3 \sin 2\alpha \ \ \varepsilon_2 \cos\alpha \right]^\top, \tag{80}$$

where $\overline{\varepsilon}_3 = \prod_{i=1}^{3} \varepsilon_i$, with ε_i being bounded positive coefficients. Assuming that $\varepsilon_1 > 0$, $\varepsilon_2 \in (0, \pi)$ and $\varepsilon_3 \in \left(0, \frac{1}{2}\right)$ one can show that the full rank condition of matrix $W(\alpha)$ is satisfied (in [20] a more general case is discussed). To design the controller, derivative $\dfrac{\partial f_T}{\partial \alpha}$ is computed in basis $X(f_T)$ as follows, [15]:

$$A_T(\alpha) := X(f_T)^{-1} \frac{\partial f_T}{\partial \alpha} \in \mathbb{R}^3. \tag{81}$$

Next, we assume that a difference between g_v and configuration of the controlled robot, g, is determined by function f_T as

$$f_T = g_v^{-1} g. \tag{82}$$

Equivalently, one can write that $g_v = g f_T^{-1}$. Taking time derivative of g_v one obtains the following dynamics

$$\dot{g}_v = X(g_v) Ad^X(f_T) \overline{C}(\alpha) \overline{u}, \tag{83}$$

where

$$\overline{u} := [u^\top \ \dot{\alpha}]^\top \in \mathbb{R}^3, \tag{84}$$

$\overline{C}(\alpha) := [C \quad -A_T(\alpha)] \in \mathbb{R}^{3\times 3}$, while $Ad^X(h) := X(e)^{-1} \ Ad(h) X(e)$, and $Ad(h) := \dfrac{d}{d\sigma}(h\sigma h^{-1})|_{\sigma=e}$, $h \in G$ defines the adjoint operator which describes the action of group G on its own algebra $\mathfrak{g}$.

As a result of transversality condition, $\overline{C}$ is the invertible matrix and dynamics (83) can be fully decoupled by applying the following dynamic feedback

$$\overline{u} = \overline{C}^{-1}(\alpha) Ad^X(f_T^{-1}) \eta, \tag{85}$$

where η is the input computed by the navigation algorithm according to formula (17).

The presented controller gives possibility to track any bounded trajectory g_v with an arbitrarily accuracy dependent on the selection of parameters of transverse function f_T. Similarly, one can state that system (6) is decoupled approximately.

The structure of the proposed control system is depicted in Fig. 5. It can be seen that the navigation algorithm computes velocity η based on (17) taking into account configuration g_v of the virtual omnidirectional robot. This configuration is determined for current configuration g of the unicycle-like robot. Signal η is then mapped on feasible control input u.

Investigating properties of algorithm (85) one can analyse how particular components of η are transformed to inputs u_1, u_2. Assuming that $A_T \in \mathbb{R}^3$ is composed of two terms $A_{T_1} \in \mathbb{R}^2$ and $A_{T_2} \in \mathbb{R}$, taking into account the structure of matrix $\overline{C}$, and computing inverse of $\overline{C}$ one can rewrite (85) as follows

$$u = \left[I \ -A_{T_1} A_{T_2}^{-1} \right] Ad^X(f_T^{-1}) \eta. \tag{86}$$

Next, in order to simplify considerations, it is assumed that norm $\|f_T\|$ is small enough such that $Ad^X(f_T^{-1})$ can be approximated by the identity matrix (notice

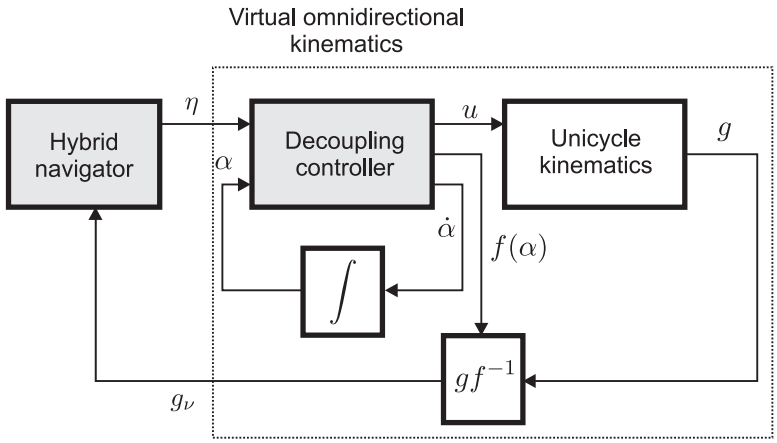

Figure 5: Diagram of the proposed control system

that from definition of Ad one has: $Ad(e) = I$). Consequently, one can consider the following approximation

$$u \approx \begin{bmatrix} \eta_1 \\ \eta_2 \end{bmatrix} - A_{T_1} A_{T_2}^{-1} \eta_3. \tag{87}$$

From (87) follows that input η_3 is multiplied by term $A_{T_1} A_{T_2}^{-1}$, which can be adjusted by a proper selection of transverse function parameters. Referring to [20] one can prove that $A_{T_1} A_{T_2}^{-1}$ is bounded as follows: $\|A_{T_1} A_{T_2}^{-1}\| \leqslant \dfrac{L}{\min\{\varepsilon_1, \varepsilon_2\}}$, where $L > 0$ is some constant. Accordingly, one can expect that η_3 is amplified significantly for small ε_1 and ε_2. Taking into account this aspect, infeasible velocity η_3 for the unicycle kinematics should be restricted during holonomic navigation. Otherwise the control algorithm (85) can produce high-magnitude inputs u_1 and u_2, which might be too restrictive in many applications.

6. Simulation and experimental results

6.1. Simulations

In order to verify the proposed concept of robust navigation, simulations in Matlab/Simulink environment were conducted. It was assumed that the measurement of configuration are corrupted by the uniform noise with amplitude equals to 0.02 m (position) and 0.05 rad (orientation).

Vector fields Y_h and Y_{nh} are defined by (70) and (72), respectively with $k_\nu = 1$, $\beta_\nu = 1.2$, $\kappa_\nu = \pm 1$ and $k_\theta = 4$.

Simulations S1 and S2 are restricted to the navigation algorithm presented in section 3.2. The initial condition is selected as $g_V(0) = [0\ 5\ 0]^\top$. In S1 only the nonholonomic mode is employed while in S2 the smooth switching between two types on navigation methods is used with parameters $c_p = 0.5$, $r_p = 0.2$, $c_\theta = 0.2$ and $r_\theta = 0.1$.

Comparing the time response of the closed-loop system (Figs. 6a, b and 7a, b), one can confirm the lack of robustness when the pure nonholonomic navigation feedback is used. Standard deviations of input signals η_1 (longitudinal velocity) and η_2 (angular velocities) computed in time range $t \in (10, 20]$ s are given as follows: $\sigma_{\eta_1} \approx 0.012$ m/s, $\sigma_{\eta_2} \approx 6.25$ rad/s for S1 and $\sigma_{\eta_1} \approx 0.011$ m/s, $\sigma_{\eta_2} \approx 0.11$ rad/s for S2. Following these data, one can conclude that the hybrid navigation algorithm provides much higher level of robustness to an additive measurement noise in a neighbourhood of the desired point. Analysing Fig. 7c it can be observed that function V decreases almost from the initial time instant (additional effects introduced by the simulated noise are neglected here). Error $\widetilde{\theta}_V$, which describes a measure of the trajectory compatibility with phase constraint (5), tends to zero. In Fig. 7d the transient phase between nonholonomic and holonomic navigation is illustrated. From time plot of V it can be seen that the navigation strategy is changed continuously without chattering effect.

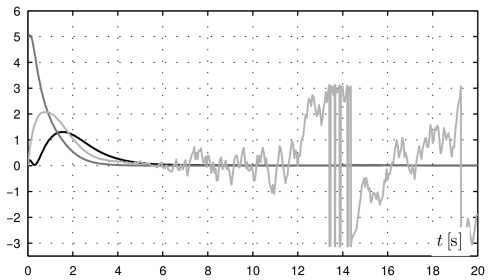

(a) Configuration: x_V (■), y_V (■) [m], θ_V (■ in [rad])

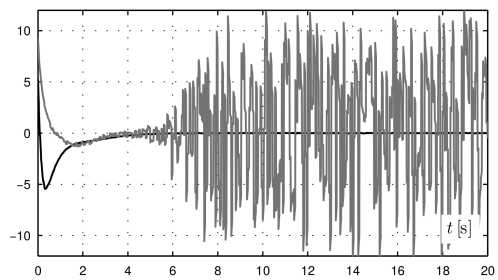

(b) Velocity: η_1 (■) [m/s], η_2 (■) [rad/s]

Figure 6: Results of simulation S1

In simulations S3 and S4 the navigation structure with decoupling controller is investigated. Parameters of the transverse function are chosen as follow: $\varepsilon_1 = 0.2$, $\varepsilon_2 = 0.15$ and $\varepsilon_3 = 0.25$. Simulations were conducted for various initial conditions. In S3 switching functions σ_{c_p,r_p} and $\sigma_{c_\theta,r_\theta}$ are parametrized in the same way as in simulations S1 and S2. In S4 the phase transition is strongly increased by assuming the following set of parameters: $c_p = 5$, $r_p = 2.5$, $c_\theta = 2$ and $r_\theta = 1$. In Fig. 8 position trajectories p are presented. Based on these results, it can be noticed that for simulation S3 trajectories converge to the switching set in such a way that no significant violation of nonholonomic constraint is required by the holonomic navigator near the origin. This is due to property of the nom-

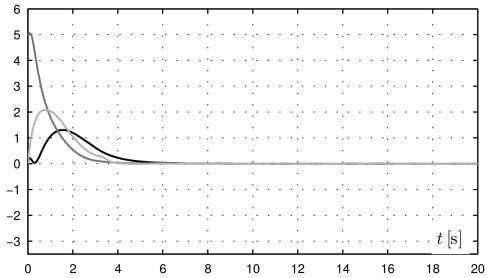

(a) Configuration: x_v (■), y_v (■) [m], θ_v (■ in [rad])

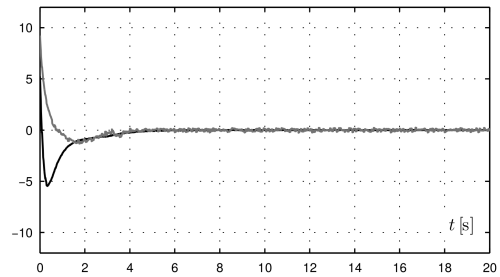

(b) Velocity: η_1 (■) [m/s], η_2 (■) [rad/s]

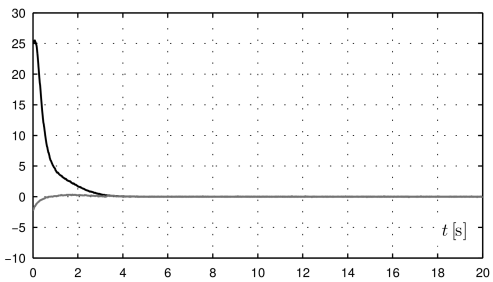

(c) Auxiliary errors: V (■) and $\widetilde{\theta}_v$ (■) [rad]

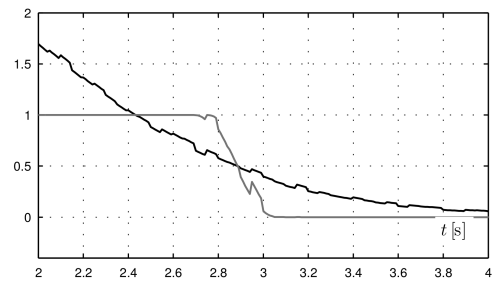

(d) Transient phase: V (■) and switching function σ_{c_p,r_p} (■)

Figure 7: Results of simulation S2

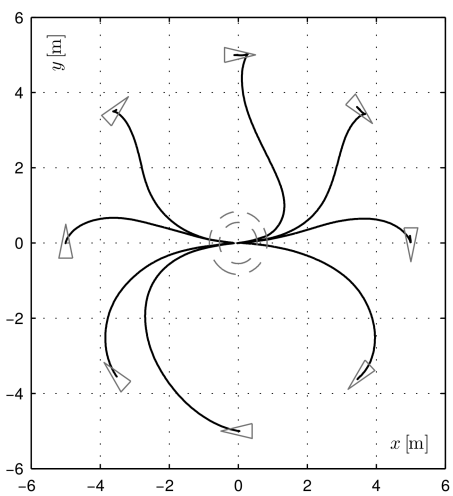

(a) Simulation S3

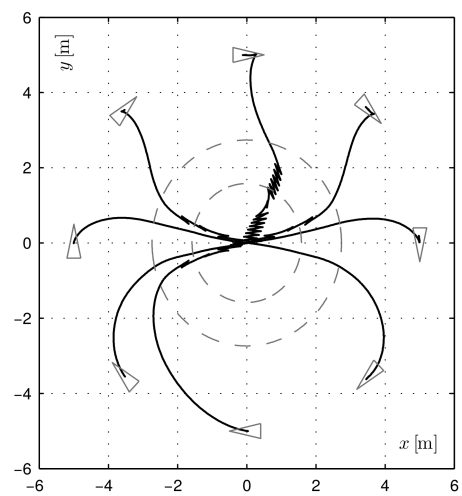

(b) Simulation S4

Figure 8: Paths obtained in simulations S3 ans S4 for the selected initial conditions – the switching area is marked by two circles

inal nonholonomic vector field (cf. assumption A4) for which integral curves are tangent to X_G-axis of the inertial frame at the origin. Conversely, when the transient area is increased similarly as in simulation S4, the discussed effect is less visible. In such a case the trajectories are not yet directed toward the desired point when the holonomic navigation algorithm becomes predominant. As a result, in a vicinity of the origin the navigator can produce infeasible trajectory g_v which has to be approximated by the unicycle.

In Figs. 9 and 10 exemplary time plots obtained in simulations S3 and S4, respectively, for initial condition $g(0) = [0\ 5\ 0]^\top$ are depicted. The steady-state error basically comes from the selected parameters of the transverse function and is bounded as follows: $|x| < 0.2$ m, $|y| < 0.0075$ m and $|\theta| < 0.15$ rad. Standard deviations of input signals u_1 and u_2 are: $\sigma_{u_1} \approx 0.19$ m/s, $\sigma_{u_2} \approx 0.11$ rad/s. From Fig. 10 it can be seen that during transient phase trajectory g_v becomes highly infeasible (cf. approximated formula (87)). Such a trajectory has to be approximated in oscillatory way that increases energy effort considerably. However, frequency of these oscillations can easily limited by a proper scaling of η. This method was applied during experimental research.

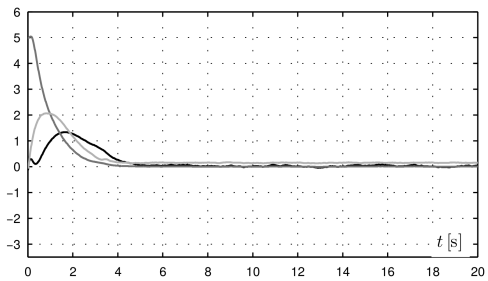

(a) Configuration of the robot: x (■), y (■) [m], θ (■ [rad])

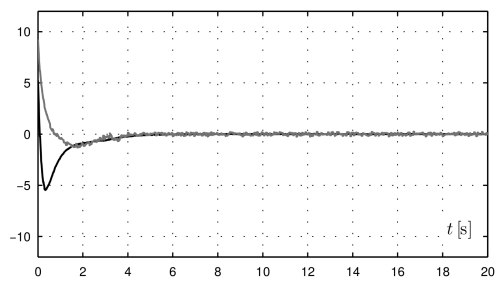

(b) Control inputs: u_1 (■) [m/s], u_2 (■) [rad/s]

Figure 9: Results of simulation S3

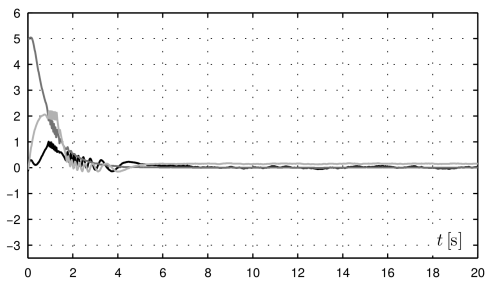

(a) Configuration of the robot: x (■), y (■) [m], θ (■ [rad])

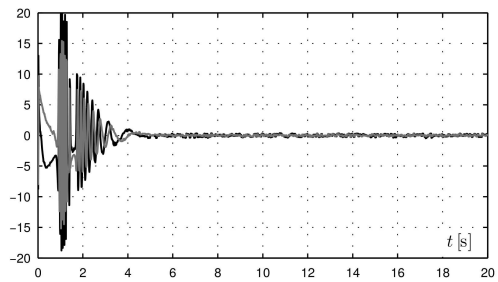

(b) Control inputs: u_1 (■) [m/s], u_2 (■) [rad/s]

Figure 10: Results of simulation S4

6.2. Experimental verification

In order to verify properties of the motion controller with the proposed navigation method, experimental work was conducted using a laboratory two-wheeled robot MTracker [8]. The algorithm was implemented in Matlab and the controller was connected to the robot taking advantage of a software driver written in C++. Frequency of the control loop was equal to 50 Hz. The robot was localized using the odometry.

To limit magnitude of control inputs, navigation velocity η was scaled using the following formula

$$\eta_s = \frac{1}{s}\eta, \tag{88}$$

where $s = \max\left\{1, \frac{\eta_1}{\overline{\eta}_1}, \frac{\eta_2}{\overline{\eta}_2}, \frac{\eta_3}{\overline{\eta}_3}\right\}$ and η_i $(i = 1,2,3)$ denotes maximum magnitude of the corresponding component η_i. In experiments the following bounds were selected: $\overline{\eta}_1 = 0.4$, $\overline{\eta}_2 = 1.0$ and $\overline{\eta}_3 = 0.03$.

The measurement uncertainties came from the odometry as well as from the additive uniform noise with the amplitude equal to 0.002 m (position) and 0.005 rad (orientation). The parameters of the navigation algorithm was set as follows: $k_v = 1$, $\beta_v = 1.2$ and $\kappa_v = 1.8$. The transverse function was parametrized by: $\varepsilon_1 = 0.1$, $\varepsilon_2 = 0.15$ and $\varepsilon_3 = 0.25$.

In experiment E1 only nonholonomic navigation strategy was considered with initial condition $g(0) = [0\ 1\ 0]^\top$. The results presented in Fig. 11 confirm that the algorithm is not stable at the desired point – the orientation variable does not converge to an equilibrium point.

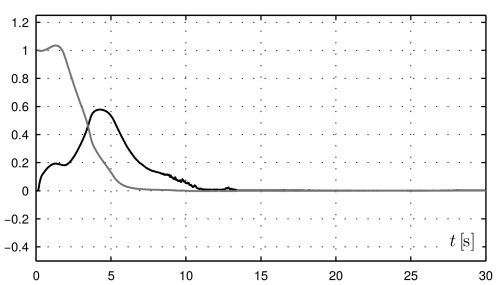

(a) Position coordinates: x (■), y (■) in [m].

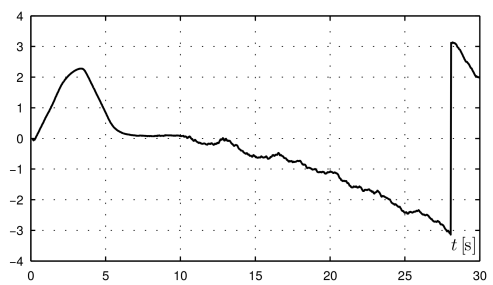

(b) Orientation θ [rad].

Figure 11: Results of experiment E1 – the control system with the nonholonomic navigator

For the comparison purpose, the pure holonomic navigation was verified in experiment E2. As indicated from Fig. 12 one can notice that the convergent rate is decreased considerably. This is due to significant limitations imposed on η_3.

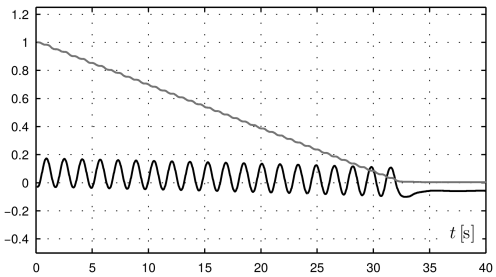

(a) Position coordinates: x (■), y (■) in [m].

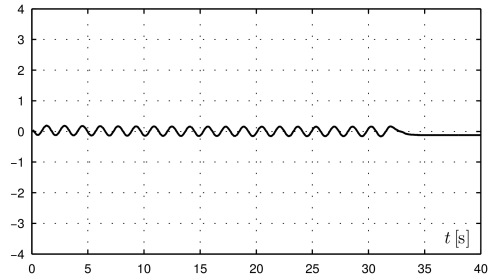

(b) Orientation θ [rad].

Figure 12: Results of experiment E2 – the control system with the holonomic navigator

In this case vector field Y_h determines strong infeasible direction in the phase space. As a result, the motion controller employs oscillatory inputs in order to approximate this direction.

In experiment E3 the proposed smooth navigation strategy was employed with the following parameters of switching functions: $c_p = 0.2$, $r_p = 0.075$, $c_\theta = 0.1$ and $r_\theta = 0.025$. From Fig. 13 one can conclude that the last strategy gives the best results, namely it ensures short regulation time, provides no oscillatory

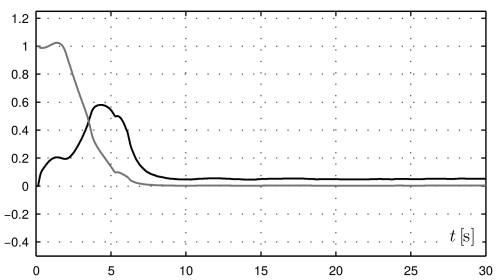

(a) Position coordinates: x (■), y (■) in [m].

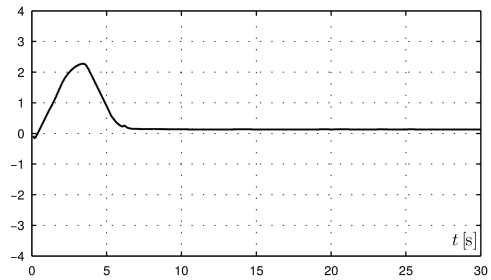

(b) Orientation θ [rad].

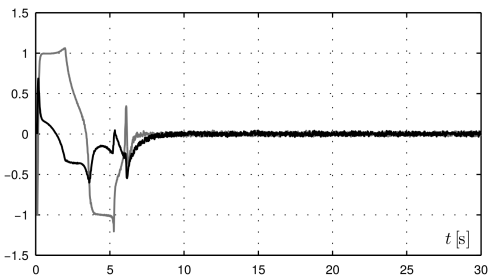

(c) Control inputs: u_1 (■) [m/s] , u_2 (■) [rad/s].

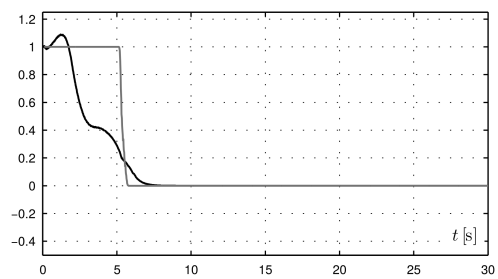

(d) Functions V (■) and σ_p (■)

Figure 13: Results of experiment E3 – the control system with the smooth robust navigator

response of the closed-loop system and guarantees sufficient level of robustness to disturbances.

Additionally, in Fig. 14 paths obtained in the experiments can be compared.

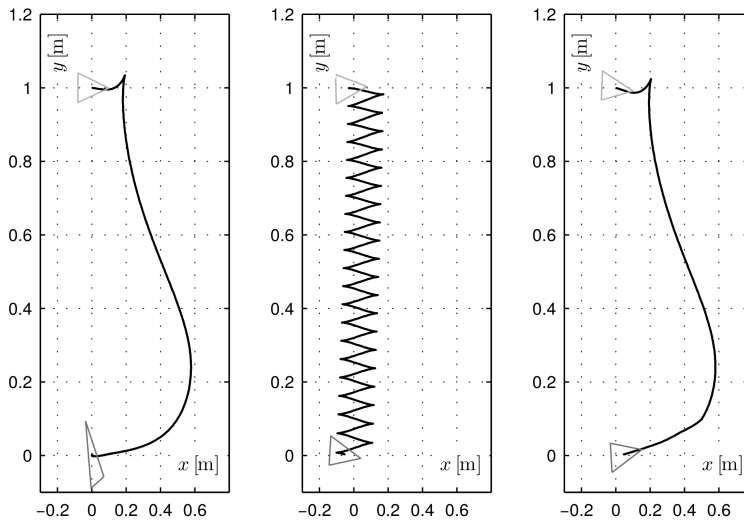

(a) Experiment E1 (b) Experiment E2 (c) Experiment E3

Figure 14: Robot paths obtained in experiments E1, E2 and E3

7. Conclusions

The control algorithm discussed in this paper consists of the smooth navigation feedback (locally imposing holonomic strategy) and decoupling controller taking advantage of transverse functions. The proposed control structure is dedicated to robots with unicycle-like kinematics. The algorithm is formally analysed in details and the stability proof of the closed-loop dynamics taking into account the controller robustness to unmodeled disturbances is discussed.

Additionally, it is worth mentioning that the proposed navigation technique can be applied also for the trajectory tracking, especially when reference velocities become slow. In such a case the uniform control strategy based on transverse functions provides a quite natural way to ensure stability around a fixed point or time-varying trajectory.

The author also believes that the presented approach can be efficiently extended to more complicated kinematics (including, for example, car-like kinematics – cf. preliminary results in [22]) for which a simple decomposition of position and orientation control cannot be accomplished directly.

In order to improve stabilization accuracy it also possible to apply another class of transverse functions which allows one to conditionally obtain the asymptotic stability – cf. [17, 21].

A. Appendix

A.1. Derivative of an angle

Let μ_1 and μ_2 be real-valued C^1 class functions. Define

$$\varphi = \operatorname{atan2}(\mu_2, \mu_1) \in \mathbb{S}^1. \tag{89}$$

Derivative $\dfrac{d}{ds}\varphi$, where $s \in \mathbb{R}$ is independent parameter can be computed as follows

$$\frac{d}{ds}\varphi = \frac{1}{\mu_1^2 + \mu_2^2}\left(\mu_1 \frac{d\mu_2}{ds} - \mu_2 \frac{d\mu_1}{ds}\right). \tag{90}$$

Defining $\mu := [\mu_1 \;\; \mu_2]^\top$ and $J := \begin{bmatrix} 0 & 1 \\ -1 & 0 \end{bmatrix}$ Eq. (91) can be rewritten as

$$\frac{d}{ds}\varphi = \frac{\mu^\top}{\|\mu\|^2} J \frac{d}{ds}\mu. \tag{91}$$

A.2. Sensitivity of angle variable

Consider constants $\overline{\mu}_1$ and $\overline{\mu}_2 \in \mathbb{R}$ and independent variable $\gamma \in \mathbb{R}$. Redefine φ from (89) as follows

$$\varphi = \operatorname{atan2}(\mu_2 + \gamma\overline{\mu}_2, \mu_1 + \gamma\overline{\mu}_1) \in \mathbb{S}^1 \tag{92}$$

and compute the following derivative

$$\frac{\partial\varphi}{\partial\gamma} = \frac{\overline{\mu}_2(\mu_1 + \gamma\overline{\mu}_1) - \overline{\mu}_1(\mu_2 + \gamma\overline{\mu}_2)}{(\mu_1 + \gamma\overline{\mu}_1)^2 + (\mu_2 + \gamma\overline{\mu}_2)^2}. \tag{93}$$

Alternatively, assuming that $\overline{\mu} = [\overline{\mu}_1 \;\; \overline{\mu}_2]^\top$ and recalling (91) one can obtain

$$\frac{\partial\varphi}{\partial\gamma} = \frac{(\mu + \gamma\overline{\mu})^\top}{\|\mu + \gamma\overline{\mu}\|^2} J\overline{\mu}. \tag{94}$$

References

[1] M. K. BENNANI and P. ROUCHON: Robust stabilization of flat and chained systems. In *Proceedings of the Third European Control Conference*, pp. 2642–2646, Rome, 1995.

[2] R.W. BROCKETT: Asymptotic stability and feedback stabilization. In R. W. Brockett, R. S. Millman, and H. J. Sussmann, editors, *Differential Geometric Control Theory*, pp. 181–191. Birkhäuser, Boston, 1983.

[3] I. DULĘBA: *Algorithms of motion planning for nonholonomic robots*. Oficyna Wydawnicza Politechniki Wrocławskiej, Wrocław, 1998.

[4] L. GURVITS and Z.X. LI: Smooth time-periodic feedback solutions for nonholonomic motion planning. In *Nonholonomic motion planning*, pp. 53–108. Kluwer, 1993.

[5] J. P. HESPANHA, D. LIBERZON and A.S. MORSE: Logic-based switching control of a nonholonomic system with parametric modeling uncertainty. *Systems and Control Letters*, **38** (1999), 167–177.

[6] B. JAKUBCZYK: Nonholonomic path following with fastly oscillating controls. In *Proc. 9th Int. Workshop on Robot Motion and Control (RoMoCo)*, pp. 99–103, 2013.

[7] Z.-P. JIANG: Robust exponential regulation of nonholonomic systems with uncertainties. *Automatica*, **36** (2000), 189–209.

[8] K. KOZŁOWSKI, W. KOWALCZYK, B. KRYSIAK, M. KIEŁCZEWSKI and T. JEDWABNY: Modular architecture of the multi-robot system for teleoperation and formation control purposes. In *Proc. 9th Int. Workshop Robot Motion and Control (RoMoCo)*, pp. 19–24, Wąsowo, Poland, July 2013.

[9] G. LAFFERRIERE and H. SUSSMANN: Motion planning for controllable systems without drift. In *Proc. of the IEEE Int. Conf. on Robotics and Automation*, pp. 1148–1153, 1991.

[10] D.A. LIZÁRRAGA, P. MORIN and C. SAMSON: Non-robustness of continuous homogeneous stabilizers for affine control systems. In *Proc. 37th IEEE Conf. on Decision and Control*, pp. 855–860, Phoenix, USA, 1999.

[11] G.A.D. LOPES and D.E. KODITSCHEK: Level sets and stable manifold approximations for perceptually driven nonholonomically constrained navigation. In *Proc. IEEE/RJS International Conference on Robotics and Systems*, pp. 1481–1486, 2004.

[12] M. MICHAŁEK and K. KOZŁOWSKI: Vector-Field-Orientation feedback control method for a differentially driven vehicle. *IEEE Trans. Control Syst. Technol.*, **18**(1) (2010), 45–65.

[13] M. MICHAŁEK and D. PAZDERSKI: A hybrid robust stabilizer for mobile robot with (2,0) kinematics. In *Prace naukowe, Elektronika z. 175*, pp. 391–400. Oficyna Wydawnicza Politechniki Warszawskiej, 2010.

[14] P. MORIN and C. SAMSON: Robust stabilization of driftless systems with hybrid open-loop/feedback control. In *Proceedings of the American Control Conference*, pp. 3929–3933, Chicago, Illinois, 2000.

[15] P. MORIN and C. SAMSON: Practical stabilization of driftless systems on Lie groups: the transverse function approach. *IEEE Trans. Autom. Control*, **48**(9) (2003), 1496–1508.

[16] P. MORIN and C. SAMSON: Trajectory tracking for non-holonomic vehicles: overview and case study. In *Proceedings of the 4th International Workshop On Robot Motion and Control*, pp. 139–153, Puszczykowo, 2004.

[17] P. MORIN and C. SAMSON: Control of nonholonomic mobile robots based on the transverse function approach. *IEEE Trans. Robot.*, **25**(5) (2009), 1058–1073.

[18] G. ORIOLO, A. DE LUCA and M. VENDITTELI: WMR control via dynamic feedback linearization: design, implementation and experimental validation. *IEEE Trans. Control Syst. Technol.*, **10**(6) (2002), 835–852.

[19] D. PANAGOU, H.G. TANNER and K.J. KYRIAKOPOULOS: Control design for a class of nonholonomic systems via reference vector fields and output regulation. *J. Dyn. Syst-T ASME*, **137**(8) (2015), 378–400.

[20] D. PAZDERSKI: Application of transverse functions to control differentially driven wheeled robots using velocity fields. *Bull. Pol. Ac.: Tech.*, **64**(4) (2016), 831–851.

[21] D. PAZDERSKI: Waypoint following for differentially driven wheeled robots with limited velocity perturbations. Asymptotic and practical stabilization using transverse function approach. *J. Intell. Robotic Syst.*, **85**(3) (2017), 553–575.

[22] D. PAZDERSKI and K. KOZŁOWSKI: Motion control of a car-like vehicle with front driving wheels using an approximate decoupling based on the transverse function approach. In *Proc. 11th Int. Workshop on Robot Motion and Control (RoMoCo)*, pp. 154–159, 2017.

[23] D. PAZDERSKI, B. KRYSIAK and K. KOZŁOWSKI: A comparison study of discontinuous control algorithms for three-link nonholonomic manipulator. In *Lecture Notes in Control and Inform. Sci. Robot Motion Control: Recent Developments*, volume 396, pp. 35–44. Springer-Verlag, Berlin Heidenberg, 2012.

[24] J.-B. POMET, B. THUILOT, G. BASTIN and G. CAMPION: A hybrid strategy for the feedback stabilization of nonholonomic mobile robots. In *Proceedings of the 1992 IEEE International Conference on Robotics and Automation*, pp. 129–134, Nice, France, 1992.

[25] C. PRIEUR and A. ASTOLFI: Robust stabilization of chained systems via hybrid control. *IEEE Transactions on Automatic Control*, **48**(10) (2003), 1768–1772.

[26] E. VALTOLINA and A. ASTOLFI: Local robust regulation of chained systems. *Systems and Control Letters*, **49** (2003), 231–238.

[27] A. ZUYEV: Exponential stabilization of nonholonomic systems by means of oscillating controls. *SIAM J. Control Optim.*, **54**(3) (2016), 1678–1696.